DOI:10.25092/baunfbed. 1823759 *J. BAUN Inst. Sci. Technol., 28(1), 435-448, (2026)*

Numerical investigation of propeller flow field using mrf model

Abdelrahman A. Mahir [1], Ayşe YÜKSEL OZAN [2,*]

[1]*Aydın Adnan Menderes University, Graduate School of Natural and Applied Sciences, Aydın.*
[2]*Aydın Adnan Menderes University, Civil Engineering Department, Aydın.*

Geliş Tarihi (Received Date): 14.11.2025
Kabul Tarihi (Accepted Date):07.01.2026

Abstract

This research employs computational fluid dynamics to examine the velocity field and bed shear stress produced by a propeller jet. A steady-state MRF approach was utilized to approximate the propeller's swirling. 10 inflation layers were applied at both the propeller and the seabed to better enhance the resolution of the near-wall gradients. Model sensitivity to turbulence-model selection was evaluated by testing the SST and the realizable k-ε models. The findings indicated that both models effectively simulated the overall jet structure and shear footprint, yet they exhibited differences in detail: the k-ε model estimated a higher shear stress value of ~0,11 Pa with a broader scour pattern, whereas the SST model maintained a narrower jet core and a more concentrated vortex with shear stress maxima of ~0,078 Pa. The results indicate the importance of selecting appropriate mesh configurations and turbulence models for accurately predicting propeller jet scours.

Keywords: *Propeller jet, Wall shear stress, CFD, Turbulence modelling.*

Pervane akım alanının mrf modeli ile sayısal analizi

Öz

Bu araştırma, hesaplamalı akışkanlar dinamiğini kullanarak pervane jeti ile oluşan hız alanı ve taban kayma gerilimesini incelemektedir. Pervanenin çevri hareketini yaklaşık olarak hesaplamak için kararlı akım koşullarında MRF yaklaşımı kullanılmıştır. Taban yakınındaki sınır tabakası çözünürlüğünü daha iyi elde edebilmek için hem pervaneye hem de tabana 10 kademeli çözüm ağı uygulanmıştır. Türbülans modelinin duyarlılığı, SST ve gerçekleştirilebilir k-ε modellerini test ederek değerlendirilmiştir. Bulgular, her iki modelin de genel jet yapısını ve taban kayma gerilmesi izini etkili bir şekilde

[*] Ayşe YÜKSEL OZAN, ayse.yuksel@adu.edu.tr, https://orcid.org/0000-0003-1931-3528
Abdelrahman A. Mahir, 2211900102@stu.adu.edu.tr, https://orcid.org/0009-0005-1796-2681

benzeştirdiğini, ancak ayrıntılarda farklılıklar gösterdiğini ortaya koymuştur: k-ε modeli, daha geniş bir oyulma modeliyle ~0,11 Pa'lık daha yüksek bir kayma gerilimi değeri elde ederken, SST modeli daha dar bir jet çekirdek alanı ile daha yoğun bir çevri bölgesi ve ~0,078 Pa'lık maksimum kayma gerilimi belirlemiştir. Sonuçlar pervane jeti kaynaklı oyulmalarını doğru bir şekilde belirlemek için uygun ağ konfigürasyonları ve türbülans modellerinin seçilmesinin önemini göstermektedir.

Anahtar Kelimeler: *Pervane jeti, Taban kayma gerilmesi, HAD, Türbülans modelleme.*

1. Introduction

Scour remains one of the major challenges in ensuring the stability and longevity of hydraulic structures. It occurs when there is an increase in the local sediment transport capacity around a structure placed in a river or marine environment. The importance of studying scours comes from how they pose a threat to the stability of hydraulic structures for civil engineers. Structures such as bridges, culverts, pipelines, and offshore structures are all subject to currents, waves, or a combination of both that endangers the safety and durability of the structure [1, 2].

When ships move around in open or confined waters, the generated flow from their propellers induces sediment transport and, over time, causes localized erosion. Scour is a process that frequently occurs in port basins, near quay walls, and around navigation channels, especially with the recent trend towards bigger and stronger ships [3, 4].

Propeller jets are complex with strong radial and tangential components, generating vortices, downflow zones and asymmetric shear stress patterns. These flow features are critical for initiating sediment entrainment and eventually a scour [4, 5].

For the last few decades, both experimental and numerical studies were conducted in order to study propeller jets and their caused scour [5-8]. Experiments provide significant insights into flow behaviour, yet they frequently encounter measurement limitations in proximity to the seabed, where the most crucial interactions occur. Numerical simulations, especially with the advent of sophisticated CFD tools, have offered an alternative method to show in detail the near-bed velocity and shear stress fields with enhanced precision. Nevertheless, simulating the complete three-dimensional turbulence structure adjacent to the bed continues to be a challenging endeavour, with results significantly influenced by the chosen turbulence model and the established boundary conditions.

In this context, the current study concentrates on the numerical analysis of the velocity field and shear stress distribution produced by a ship propeller in an open, unconfined environment. The complete propeller geometry is simulated using the Moving Reference Frame (MRF) technique in steady-state conditions. The realizable k-ε model and the SST k-ω turbulence models are compared on how they simulate jet propeller as well as the shear stress near the bed.

1.1. Problem statement and scope

A persistent challenge is forecasting the distribution of bed shear stress and near-bed velocity fields, both of which are keys to understanding the initiation of scour.

Turbulence models are often utilized in such situations, but they can yield varying results depending on the chosen model. However, direct comparisons between widely used turbulence models under identical and controlled propeller conditions are infrequent.

This study attempts to address this gap using a Moving Reference Frame (MRF) approach to simulate a fully modelled propeller in an open environment makes it possible to compare the predictions of two commonly used turbulence models for velocity profiles and shear stresses near the bed. Rather than directly modelling sediment transport processes, this study focuses on the hydrodynamic properties that precede and initiate scour development.

With this context in mind, the goals of this work are:
1. To perform steady-state CFD simulations of a full propeller-induced flow field in an unconfined domain,
2. To contrast the near-bed shear stress and velocity fields forecasted by the realizable k-ε and SST k-ω turbulence models.
The study seeks to examine the turbulence models' options in propeller jet simulations and provide insights that may enhance future scour prediction methodologies.

2. Methodology and setup

2.1. Governing approach and CFD tool

ANSYS Fluent was used for all the simulations, employing a steady-state solver to determine and compute the time-averaged flow field of the rotating propeller. The flow was computed as incompressible and three-dimensional, using two RANS-based models to model the turbulence: The Realizable k-ε model and the SST k-ω model. The core of this study is comparing these two models, which are commonly used in marine CFD applications, but they differ in how near-wall treatment and sensitivity are handled.

$$\frac{\delta u_i}{\delta t} + u_j \frac{\delta u_i}{\delta x_j} + \frac{1}{\rho}\frac{\delta p}{\delta x_i} - \frac{1}{\rho}\frac{\delta}{\delta x j_i}\left(-\overline{\rho \acute{u}_\iota \acute{u}_J}\right) + f_i = 0 \tag{1}$$

Where $u_i$is time-averaged velocity component in the ith direction, f_i represent the body force, p is total pressure, ρ is fluid density, and $-\overline{\rho \acute{u}_\iota \acute{u}_J}$ are the Reynolds Stresses. These stresses are a result of separating each variable into its mean and fluctuating parts. These terms cannot be directly calculated, which leads to what is known as the closure problem. To solve these equations, approximations such as the Boussinesq hypothesis (Equation 2) are introduced and solving these stresses is a central feature of the Reynolds-averaged Navier-Stokes (RANS) approach.

$$-\overline{\rho \acute{u}_\iota \acute{u}_J} = 2\,\mu_t S_{ij} - \frac{2}{3}\rho k \delta_{ij} \tag{2}$$

To simulate the propeller rotation, the Moving Reference Frame (MRF) was adapted. It provides a steady-state approximation for the simulation of rotating zones. Each fluid region is assigned at a rotational speed, and the governing equations are solved in relation to that moving frame. The flow in the stationary domain is governed by the Continuity and Momentum Equations (Equation 3), while the rotating domain is governed by moving

frame formulations that introduces additional Coriolis and centrifugal terms (Equation 4). An interface at the boundaries between rotating and stationary zones ensures the continuity of the flow variables across the boundary. Moreover, the MRF approach captures the instantaneous effects of rotation without needing to simulate a full transient simulation [9].

$$\frac{\partial \rho}{\partial t} + \nabla.(\rho \vec{v}) = S_m \tag{3}$$

Where ρ is density, $\vec{v}$ is absolute velocity and S_m is the mass source term.

$$\frac{\partial}{\partial t}\rho \vec{v} + \nabla.(\rho \overrightarrow{v_r} \vec{v}) + \rho[\vec{\omega} \times (\vec{v} - \overrightarrow{v_t})] = -\nabla p + \nabla.\bar{\tau} + \vec{F} \tag{4}$$

Where $\overrightarrow{v_r}$ is relative velocity, $[\vec{\omega} \times (\vec{v} - \overrightarrow{v_t})]$ is the Coriolis and centripetal accelerations term, $\vec{\omega}$ is angular velocity vector, $\bar{\tau}$ is viscous stress tensor and $\vec{F}$ is external body forces.

2.2. Propeller information

The propeller modelled in this study is based on the geometry used in the experimental work by Cihan et al. [6]. It's a four-bladed propeller with a blade area ratio of 0,6 and a pitch ratio of 1,025, a diameter (Dp) of 75 mm, and a thrust coefficient of 0,35.

The bed itself was modelled as a hydraulically rough wall, with a wall roughness height consistent with a sand material of D_{50} = 0,11 mm. This value was not intended to represent a specific experimental sediment, but rather to provide a realistic rough wall boundary while avoiding hydraulicly smooth bed assumption. No sediment transport or bed deformation was modelled, as the focus of this study remains the hydrodynamic quantities—primarily velocity and wall shear stress that are associated with erosion. Hence, the selected wall roughness serves as a numerical parameter to capture near-bed turbulence effects.

2.3. Study of mesh generation and independence

A two-stage mesh refinement study was conducted to ensure that the flow field was resolved accurately while keeping the cost of computing reasonable. The first stage focused on the propeller zone, i.e., the rotating mesh area (Figure 1). A local refinement strategy was implemented with the goal of achieving a near-surface resolution, i.e., Y^+ must be maintained below 5 to ensure precise capture of the intricate propeller flows and their impacts. The main steps were as follows:

- Rotating domain sizing: 5 mm element,
- 10 inflation layers between the propeller blades and its rotating domain,
- Propeller blade elements sizing: 1 mm on the blade surfaces,
- Curvature sizing: Set to 10° to better capture the propeller curved geometry.

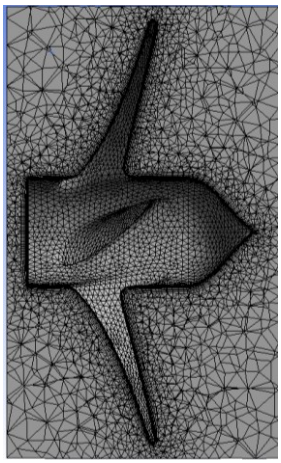

Figure 1. Propeller domain mesh - cross section (Y-Z plane)

A cross-section of computational domain is given in Figure 2.

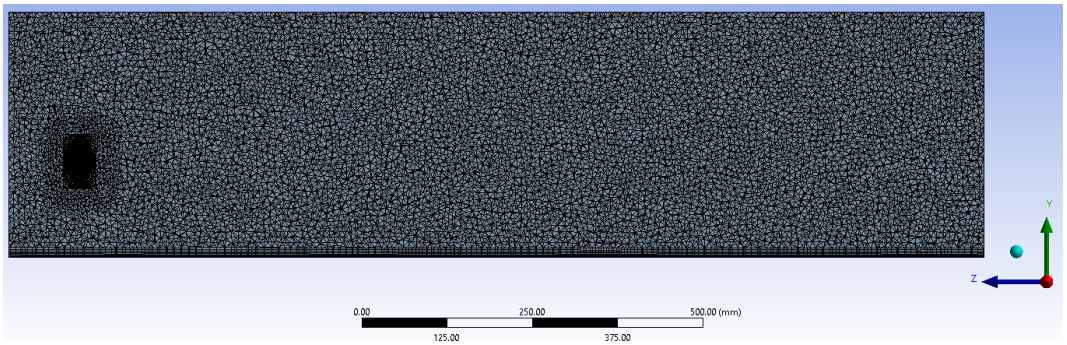

Figure 2. Computational domain mesh - cross section (Y-Z plane)

The chosen inflation settings and blade mesh resolution successfully maintained $Y^{+}< 5$ over most of the blade surfaces, supporting the validity of the local refinement strategy in the near-wall zone (Figures 3-4).

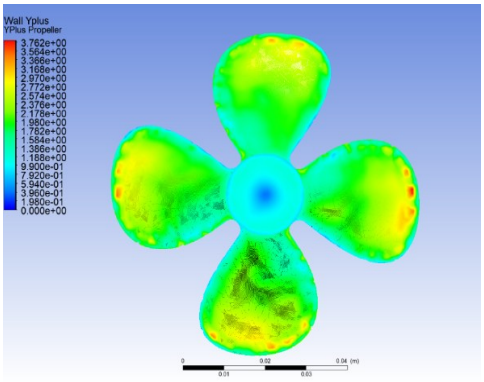

Figure 3. Propeller Y^{+} values - front view

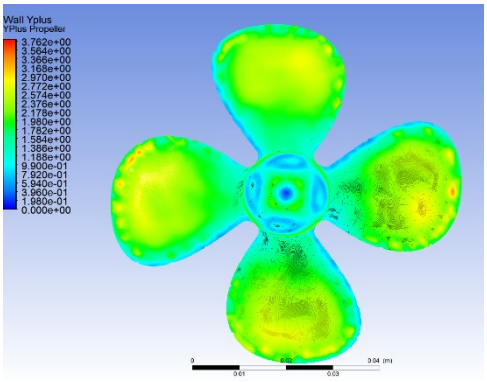

Figure 4. Propeller Y^{+} values - back view

The second stage involved a global mesh sensitivity analysis using a reduced computational domain volume to isolate the effect of mesh resolution. Propeller zone

settings were kept constant, and the global mesh element size was varied from 22,5 mm down to 7,5 mm. Velocity profiles were extracted at seven downstream locations (from 5 cm to 40 cm in front of the propeller), and the results from each mesh case were compared to those obtained with the finest mesh (7,5 mm), which served as a reference. The results indicated that, although finer meshes often enhanced the resolution of the velocity profile, the 10 mm mesh provided the optimal balance. It preserved the essential velocity features observed in the 7,5 mm case while significantly reducing runtime and memory usage (Table 1). As a result, the 10 mm mesh was selected for all subsequent simulations.

Table 1. Mesh element size - average velocity difference

Element size (mm)	5 cm	10 cm	20 cm	30 cm	40 cm
22,5	6,22%	1,06%	-1,61%	0,17%	4,38%
20	-2,23%	-3,99%	-2,61%	1,95%	3,68%
17,5	-2,98%	-1,09%	-3,42%	-1,31%	1,34%
15	-0,60%	-4,37%	4,57%	7,51%	4,11%
12,5	-0,42%	-3,65%	-3,10%	-2,11%	-3,11%
10	-0,52%	-4,90%	1,65%	2,12%	2,71%

In addition to the mesh sensitivity study, the performance of two pressure-velocity coupling algorithms—SIMPLEC and Coupled—was evaluated (Figure 5). Both solvers generated consistent velocity profiles, exhibiting minimal differences in resolution at the probing points. However, the coupled solver, which solves momentum and continuity equations simultaneously, required significantly more computational time. In contrast, the SIMPLEC solver, which is a variation of the SIMPLE method that speeds up convergence by altering the face flux correction formulation, does not require the additional memory and computational cost associated with full implicit coupling [9]. For this reason, the SIMPLEC algorithm was retained in all simulation runs due to its better computational efficiency and similar results.

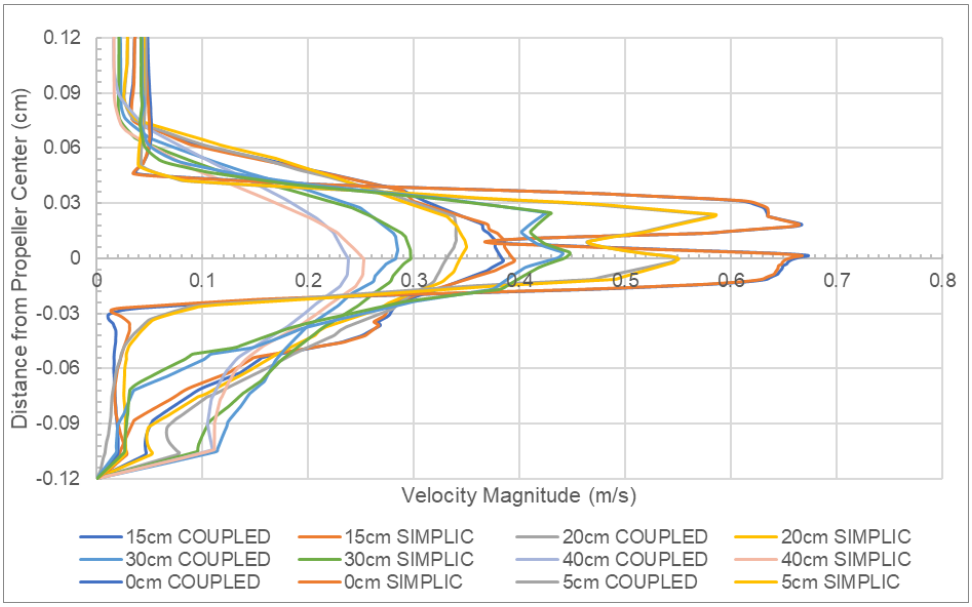

Figure 5. Velocity profile comparison SIMPLIC vs COUPLED: 0 cm – 40 cm

The efflux velocity was extracted from the numerical results at the first plane immediately downstream of the propeller's rotating zone, corresponding to the near-field exit velocity. Following the definition proposed by Lam et al. [10], the efflux velocity was taken at a distance of from the rotation axis, corresponding to $0.67(R_p - R_h)$, with R_p representing propeller radius and R_h is hub radius. This results in value = 0.63 m/s.

This value was compared against several widely used semi-empirical equations of propeller efflux velocity (Table 2). The closest agreements were obtained from the formulations recommended by PIANC [11], Fuehrer & Römisch [12] and Hamil et al. [13], which deviations less than 10%. Larger differences are observed in other formulations that incorporate geometry dependent coefficients which are calibrated for specific propeller series, blade area ratios, pitch rations and propeller diameter illustrating their inherent limitations and therefore they are not universally applicable.

Overall, the CFD efflux velocity lies within the upper bound of the semi-empirical range reported in the literature, indicating good physical consistency of the numerical model.

Table 2. Comparison of CFD efflux velocity with semi-empirical formulations

Reference Formula	Formulation	U_0 (m/s)	Difference vs CFD (%)
[12]	$1.59nD_p\sqrt{C_t}$	0.588	+7.2
[14]	$1.33nD_p\sqrt{C_t}$	0.492	+28.1
[15]	$\zeta nD_p\sqrt{C_t}$	0.541	+16.4
[13]	$1.22n^{1.01}{D_p}^{0.84}{C_t}^{0.62}$	0.614	-2.4
[16]	$1.42nD_p\sqrt{C_t}$	0.525	+16.7
Present CFD	-	0.630	-

2.4. Computation domain and boundary conditions

The domain width was set to 1000 mm (13 Dp), length to 1430 mm (19 Dp), and height to 360 mm (5 D) to minimize the confinement effects or artificial reflections of the walls on the expanding jet. The propeller was positioned at the centre of the horizontal plane with set clearance (140 mm) from the bed (Figure 6).

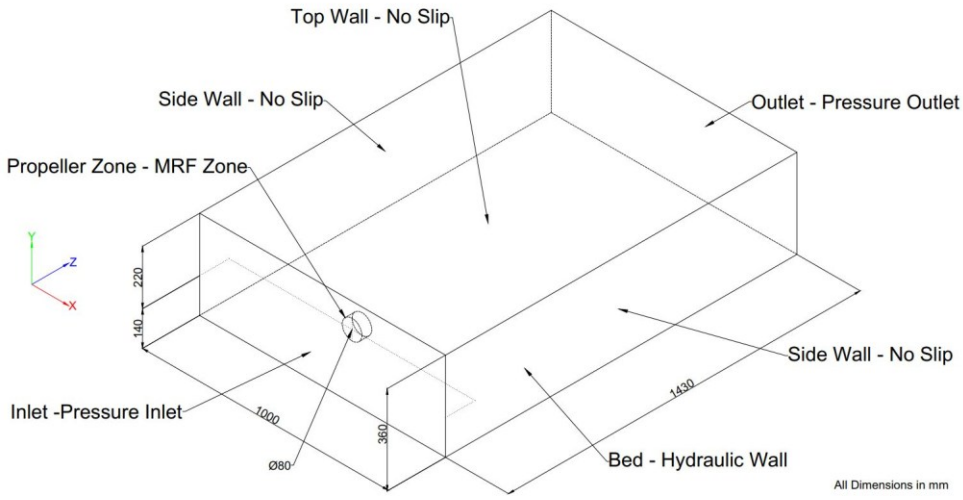

Figure 6. Computational domain and boundary conditions (all dimensions in mm)

The following boundary conditions were applied:
• Inlet: Pressure inlet, with zero initial velocity
• Outlet: Pressure outlet
• Bed: No-slip wall with roughness set to 0,11 mm
• Side and Top Walls: No-slip condition without wall roughness
• Propeller zone: MRF region with a rotational speed set to 500 RPM.

3. Results and discussion

3.1. Velocity field characteristics

Both simulations reproduce the main characteristics of a propeller jet: a high-momentum axial core that extends downstream, surrounded by regions of progressive diffusion and entrainment. Nevertheless, clear differences emerge in the degree of jet confinement, diffusion, and swirl structure predicted by the two models.

The mid-plane contours highlight the general jet development. In the SST case (Figure 7), the high-velocity core remains narrower and extends further downstream before losing intensity, whereas the realizable k-ε model (Figure 8) shows earlier lateral spread and a faster drop in peak velocity. This behaviour is consistent with the tendency of k-ε models to overpredict turbulent diffusion, resulting in broader jets and weaker axial momentum. By contrast, the SST model, which includes enhanced near-wall resolution and better handling of adverse pressure gradients, maintains a more concentrated jet.

The contracting and expanding behaviour observed in the mid-place velocity contours (Figure 7 and 8) is a characteristic feature of propeller jets and is consistent with previous experimental studies [10, 16]. In the immediate downstream region, the formation of the near-field zone of flow establishment (ZFE) is associated with contraction of the slipstream due to the axial acceleration induced by the propeller. Further downstream, the turbulent mixing and the entrainment of the surrounding fluid dominates the fluid resulting in a progressive widening of the jet and decay of its axial velocity.

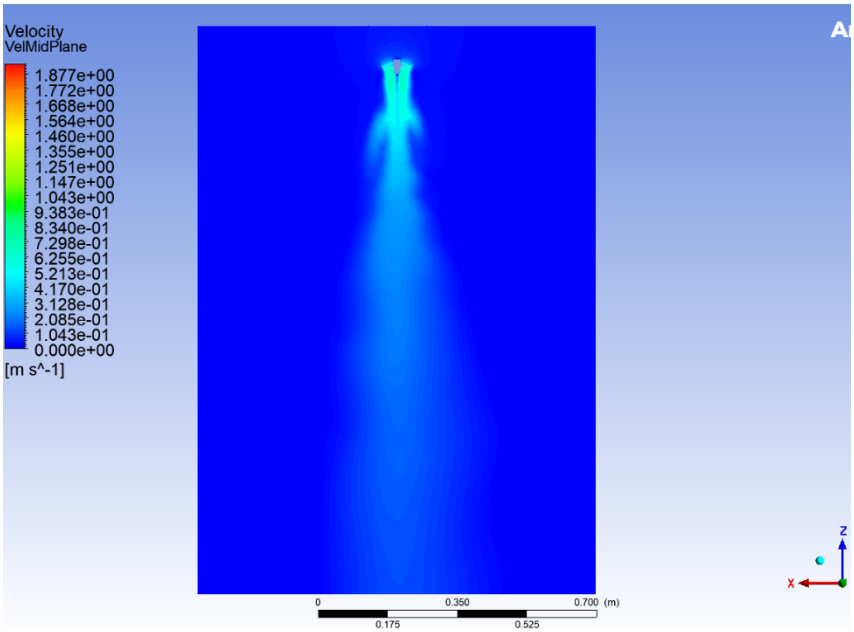

Figure 7. Velocity contour – SST model – mid plane

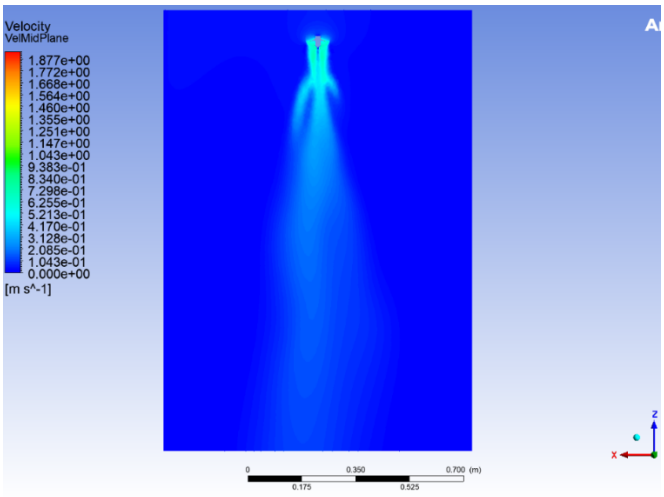

Figure 8. Velocity contour – k-ε model – mid plane

The velocity vectors close to the propeller emphasize the differences in the near field. The SST solution reveals more cohesive jet flow downstream of the blade tips and a stronger inflow towards the hub (Figure 9). In contrast, the k-ε field diffuses earlier, with velocity divergence occurring closer to the propeller plane (Figure 10). These observations reinforce the interpretation that SST retains momentum and structure more effectively in the near-propeller region.

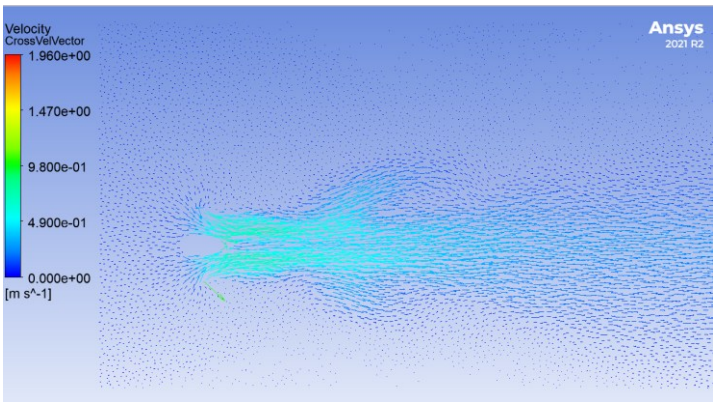

Figure 9. Near propeller velocity vectors – SST model

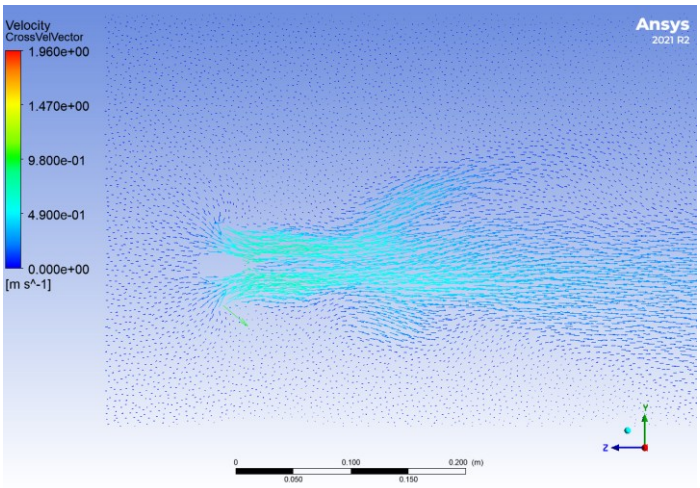

Figure 10. Near propeller velocity vectors - k-ε model

Lastly, the streamline plots further illustrate the global and swirling features of the jet. In the side view (Figure 11a), the SST streamlines remain more bonded before bending outward, whereas the k-ε streamlines spread more rapidly (Figure 12a). From the front view (Figures 11b, 12b), both models capture the formation of a swirling structure induced by propeller rotation, but the SST solution produces a more coherent central vortex, while the k-ε result is comparatively diffused. The simulated swirl is physically significant, as vortex strength and shape influence near-bed shear stresses and the initiation of scour.

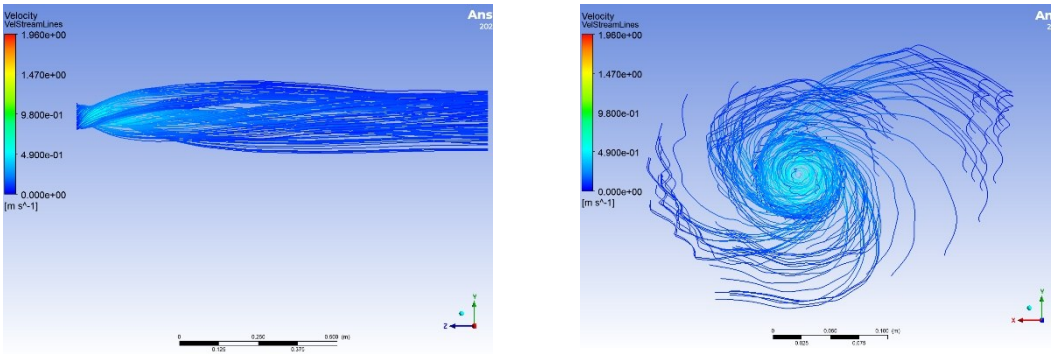

a) Side view b) Front view

Figure 11. Velocity streamlines - SST model

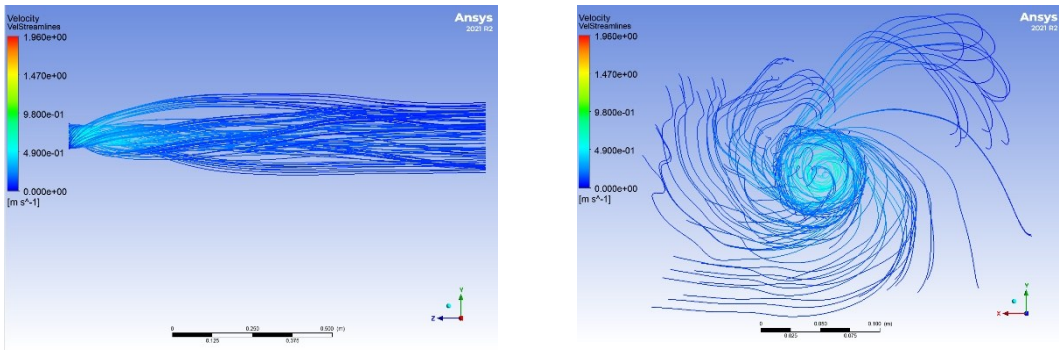

a) Side view b) Front view

Figure 12. Velocity streamlines - K-ε model

3.2. Wall shear stress distribution

Figure 13 displays the predicted bed shear stress distributions from the two turbulence models. In both cases, the main jet footprint is visible as a concentrated lobe of elevated stress, gradually spreading downstream. The maximum shear values differed between the models; the SST simulation (Figure 13a) peaked at approximately 0,078 Pa, while the realizable k-ε case (Figure 13b) reached about 0,11 Pa. The higher peak in k-ε is accompanied by a broader lateral spread, whereas SST produced a more focused footprint aligned with the jet axis.

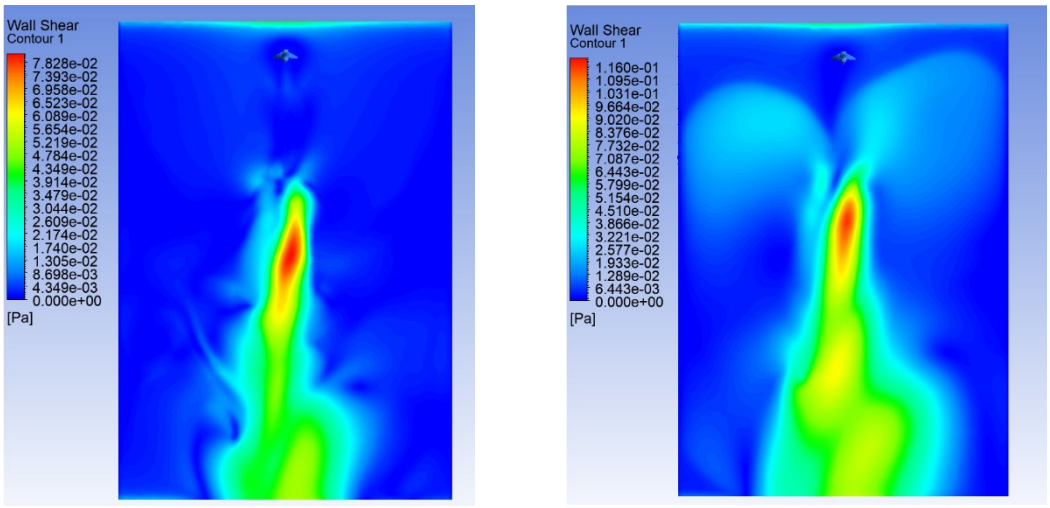

a) SST model b) K-ε model

Figure 13. Wall shear stress contour

A notable feature of the k-ε results is the presence of two symmetric lobes flanking the jet footprint. These elevated zones are not reproduced in the SST simulations and do not appear in comparable experimental studies. They are most likely artefacts linked to the use of wall functions and local numerical diffusion rather than physical shear structures.

The influence of near-wall resolution was further examined through runs with and without inflation layers (Figures 14, 15). With ten prism layers applied, Y^+ values remained below 5 on the bed (Figures 14a, 15a), enabling accurate resolution of the viscous sublayer. Under these conditions, the predicted shear stress fields were well defined, with sharper gradients and stable peak values. In contrast, the absence of inflation layers pushed Y^+ into the range of 10–20 (Figures 14b, 15b), shifting the solution into a wall-function regime. This resulted in a reduction of shear stress maximum value and noticeably fewer captured details, particularly for SST, which is formulated for low-Reynolds near-wall treatments.

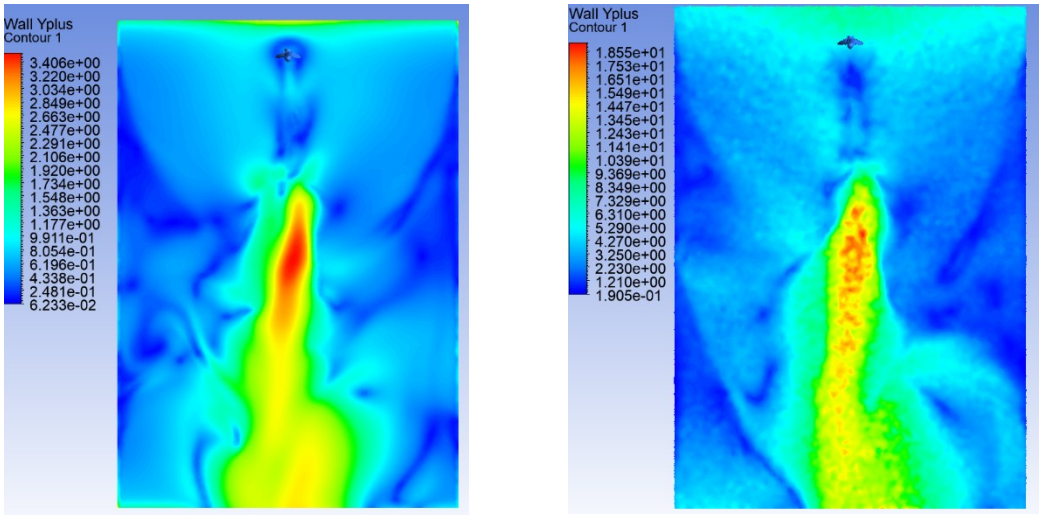

a) 10 inflation layers b) No inflation layers

Figure 14. Bed Y^+ contour - SST model

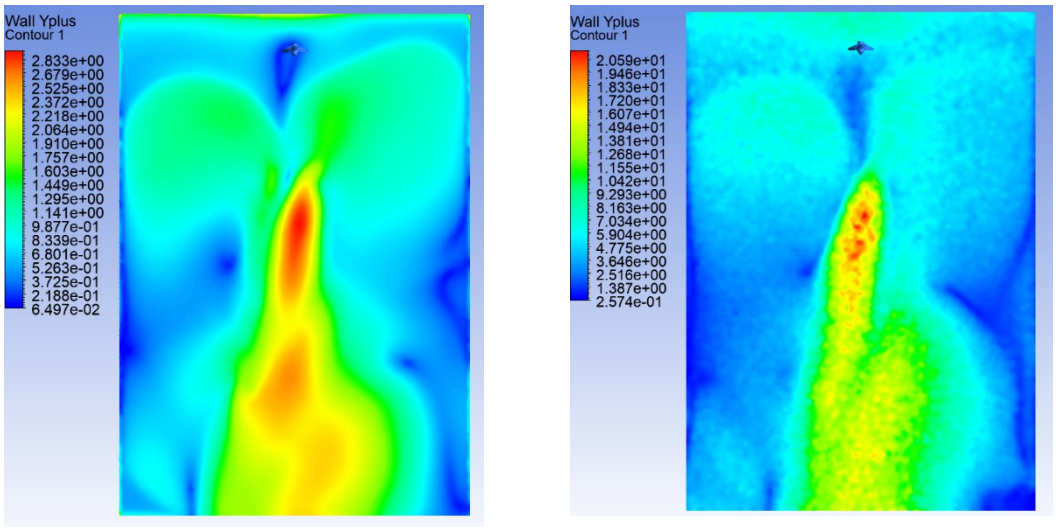

a) 10 inflation layers b) No inflation layers

Figure 15. Bed Y^+ contour - K-ε model

3.3. Turbulence model comparison

Overall, the shear stress results at the wall highlight the sensitivity of shear stress predictions to both turbulence model formulation and near-wall resolution. The inflation layer treatment was critical to maintaining physically consistent Y^+ values and producing reliable shear stress fields, while also reducing the likelihood of artificial patterns in the computed distributions.

A side-by-side assessment of the realizable k-ε and SST models shows consistent agreement on the overall jet-induced shear footprint, but with notable differences in detail. In the velocity field, SST maintained a narrower jet core and a more coherent swirl near the propeller, whereas k-ε simulated faster lateral spreading and a diminished vortex structure. This behaviour aligns with previous studies indicating that k-ε formulations, while robust, often overestimate turbulent diffusion and diminish near-field gradients. The SST model, by contrast, benefits from its near-wall k-ω formulation and shear-stress transport limiter, which reduces excessive eddy viscosity and allows sharper gradients and swirl to be retained [18].

The same tendencies were reflected in the results for bed shear stress. SST produced a more localized footprint with a maximum of about 0,078 Pa, while the realizable k-ε model predicted a broader lobe with a higher maximum of roughly 0,11 Pa. Symmetric side lobes appeared in the k-ε shear contours, which are likely numerical artefacts associated with wall functions and local mesh transitions, as they were not observed in the SST results or comparable experiments [9, 18]. Sensitivity tests further emphasized that SST requires inflation layers to maintain Y^+ below 5 and accurately resolve near-wall stresses, while k-ε was less sensitive to this refinement but showed spurious features when wall functions dominated.

Both models effectively represented the distribution of jet-induced stresses; however, they differed in terms of magnitude and spatial detail. These differences underline the strong influence of turbulence-model choice on predicting near-bed stresses, which are critical drivers of scour initiation.

4. Conclusions

This study presented a numerical investigation of the velocity field and bed shear stress generated by a ship propeller jet, with particular emphasis on turbulence-model sensitivity. Unlike simplified jet-inlet approaches, the propeller was fully modelled using an MRF formulation, allowing the swirling near-field and associated shear patterns to be directly captured. This study compared the realizable k-ε and SST models under uniform conditions, emphasizing jet development and near-bed stresses.

The results indicated that both models replicated the general pattern of the propeller jet and its associated shear effect, albeit with significant differences in detail. The SST model preserved a narrower jet core and more coherent swirl near the propeller, yielding localized shear maxima of about 0,078 Pa. The realizable k-ε model predicted higher peak stresses, around 0,11 Pa, together with a broader footprint and secondary lobes, which are likely numerical artefacts. These tendencies reflect the models' known behaviours: SST benefits from near-wall resolution and reduced eddy viscosity, while k-ε is more diffusive. Inflation layers were found to be critical in achieving consistent Y^+ levels and reliable wall shear predictions.

The study is constrained by its steady-state MRF approach, which offers a close approximation to a fully transient state yet does not achieve complete simulation accuracy, and by the absence of direct experimental validation. The observed trends are consistent with prior experimental and numerical results, underscoring the significance of turbulence-model selection in studies of propeller-jet scour. Future research should broaden the analysis to include unsteady-state conditions and integrate sediment transport through multiphase flows to enhance predictive capability.

Acknowledgement

This work was supported by the Scientific and Technological Research Council of Turkey (TUBITAK) (Project number: 218M428).

References

[1] Sumer, B. M., and Fredsøe, J. (2002). The mechanics of Scour in the marine environment. **In Advanced series on ocean engineering**. https://doi.org/10.1142/4942

[2] Transportation, U. S. D. O. (2015). Bridge scour and stream instability countermeasures: **Experience, Selection, and Design Guidance** Third Edition Volume 1.

[3] Hong, J., Chiew, Y., and Cheng, N. (2013). Scour caused by a propeller jet. **Journal of Hydraulic Engineering**, 139(9), 1003–1012. https://doi.org/10.1061/(asce)hy.1943-7900.0000746

[4] Wei, M., Chiew, Y., and Hsieh, S. (2017). Plane boundary effects on characteristics of propeller jets. **Experiments in Fluids**, 58(10). https://doi.org/10.1007/s00348-017-2425-8

[5] Tan, R. İ., and Yüksel, Y. (2018). Seabed scour induced by a propeller jet. **Ocean Engineering**, 160, 132–142. https://doi.org/10.1016/j.oceaneng.2018.04.076

[6] Cihan, K., Doğu, A., Yılmaz, D., Ozan, A. Y., Yıldız, O., and Sahin, C. (2022). Unconfined propeller jet scour on clay/sand mixtures. **Ocean Engineering**, 264, 112448. https://doi.org/10.1016/j.oceaneng.2022.112448

[7] Curulli, G., Penna, N., and Gaudio, R. (2022). Improved formulation for the geometric characteristics of the scour hole and deposition mound caused by a rotating propeller jet on a mobile bed. **Ocean Engineering**, 267, 113175. https://doi.org/10.1016/j.oceaneng.2022.113175

[8] Penna, N., D'Alessandro, F., Gaudio, R., and Tomasicchio, G. R. (2019). Three-dimensional analysis of local scouring induced by a rotating ship propeller. **Ocean Engineering**, 188, 106294. https://doi.org/10.1016/j.oceaneng.2019.106294

[9] Fluent Inc. (2003). Fluent User Manual.

[10] W. Lam, G. A. Hamill, D. J. Robinson, and S. Raghunathan, "Semi-empirical methods for determining the efflux velocity from a ship's propeller," Applied Ocean Research, vol. 35, pp. 14–24, Feb. 2012, doi: 10.1016/j.apor.2012.01.002.

[11] PIANC, Guidelines for Protecting Berthing Structures from Scour Caused by Ships. 2015.

[12] M. Fuehrer and K. Römisch, "Effects of modern ship traffic on islands and ocean waterways and their structures," in Proc. PIANC 24th Congress, Leningrad, USSR, Sep. 1977, Sections 1–3.

[13] G. Hamill, C. Kee, and D. Ryan, "Three-dimension efflux velocity characteristics of marine propeller jets," Proceedings of the Institution of Civil Engineers - Maritime Engineering, vol. 168, no. 2, pp. 62–75, Jun. 2015, doi: 10.1680/jmaen.14.00019.

[14] Hamill G.A., "Characteristics of the screw wash of manoeuvring ship and the resulting bed scour," Ph.D. thesis, Queen's University of Belfast, Northern Ireland, UK, 1987.

[15] D. P. J. Stewart, "Characteristics of a ship's screw wash and the influence of quay wall proximity," Ph.D. thesis, Queen's University of Belfast, Northern Ireland, UK, 1992.

[16] R. İ. Tan and Y. Yüksel, "Seabed scour induced by a propeller jet," *Ocean Engineering*, vol. 160, pp. 132–142, Apr. 2018, doi:10.1016/j.oceaneng.2018.04.076.

[17] M. Wei, Y.-M. Chiew, and N.-S. Cheng, "Recent advances in understanding propeller jet flow and its impact on scour," Physics of Fluids, vol. 32, no. 10, Oct. 2020, doi: 10.1063/5.0023266.

[18] Lam, W., Robinson, D., Hamill, G., and Johnston, H. (2012). An effective method for comparing turbulence intensity from LDA measurements and CFD predictions within a ship propeller jet. **Ocean Engineering**, 52, 105–124. https://doi.org/10.1016/j.oceaneng.2012.06.016